Volume 9 | Number 39 | 21 October 2018 | Pages 7577–7718

Chemical Science

rsc.li/chemical-science

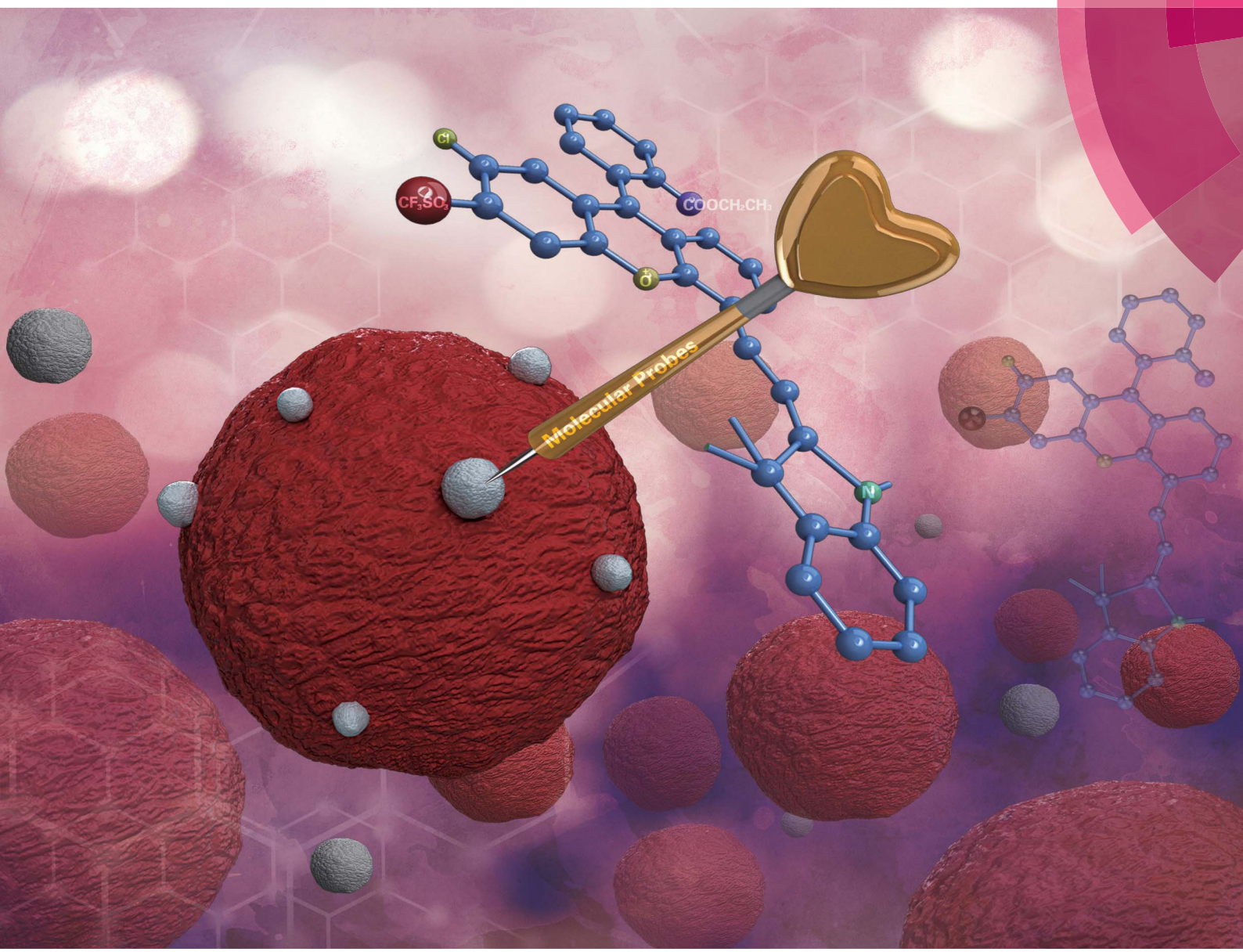

ISSN 2041-6539

ROYAL SOCIETY OF CHEMISTRY

EDGE ARTICLE

Lin Yuan *et al.*

Visualization of oxidative injury in the mouse kidney using selective superoxide anion fluorescent probes

Chemical Science

EDGE ARTICLE

View Article Online
View Journal | View Issue

Cite this: *Chem. Sci.*, 2018, **9**, 7606

All publication charges for this article have been paid for by the Royal Society of Chemistry

Visualization of oxidative injury in the mouse kidney using selective superoxide anion fluorescent probes†

Yun Lv,‡[a] Dan Cheng,‡[a] Dongdong Su,[c] Mei Chen,[d] Bin-Cheng Yin,[b] Lin Yuan*[a] and Xiao-Bing Zhang[a]

Received 26th July 2018
Accepted 10th September 2018

DOI: 10.1039/c8sc03308k

rsc.li/chemical-science

Drug-induced acute kidney injury (AKI), caused by renal drug metabolism, has been regarded as a main problem in clinical pharmacology and practice. However, due to the lack of effective biomarkers and noninvasive real-time tools, the early diagnosis of drug-induced AKI is still a crucial challenge. The superoxide anion ($O_2^{\bullet-}$), the preliminary reactive oxidative species, is closely related to drug-induced AKI. In this paper, we reported two new mitochondria-targeted fluorescent probes for investigating AKI *via* mapping the fluctuation of $O_2^{\bullet-}$ with high sensitivity and selectivity by the combination of rational design and a probe-screening approach. Small-molecule fluorescent probes (**Naph-$O_2^{\bullet-}$** and **NIR-$O_2^{\bullet-}$**) with high accuracy and excellent selectivity were successfully applied to detect endogenously produced $O_2^{\bullet-}$ in living cells and tissues by dual-model confocal imaging, and to trap the fluctuation of the $O_2^{\bullet-}$ level during the drug-induced nephrotoxicity. Moreover, probe **NIR-$O_2^{\bullet-}$** was also used to elucidate the protective effects of L-carnitine (LC) against drug-induced nephrotoxicity for the first time. Therefore, these probes may be potential chemical tools for exploring the roles of $O_2^{\bullet-}$ in complex nephrotoxicity disease systems.

Introduction

The kidney plays an essential role in metabolism and clearance of numerous hydrophilic xenobiotics and endogenous compounds.[1] As a consequence, the kidney is often exposed to drugs with high concentrations and is more susceptible to damage by drugs, which may ultimately cause acute kidney injury (AKI).[2] In fact, drug-induced AKI is a long-term concern in clinical pharmacology and accounts for 19% to 26% of cases of AKI in clinical practice,[3] which is a major reason for post-marketing withdrawals of medicinal products.[4,5] At present, serum creatinine (SCr) and blood urea nitrogen (BUN) are conventional nephrotoxicity biomarkers for the evaluation of drug-induced AKI,[6] but they are not available for early diagnosis[7,8] and usually affected by a variety of other diseases.[9] Moreover, a limited number of early biomarkers have been explored during the AKI process. For these reasons, innovative preclinical nephrotoxicity screening methods are required to evaluate early nephrotoxicity for drug development and clinical application.

Reactive oxygen species (ROS), mainly produced in mitochondria, have been revealed as the inevitable by-products in renal drug metabolism, which may lead to cell apoptosis and other acute kidney damage.[10,11] For example, cisplatin, a commonly used chemotherapeutic drug for treatment of numerous human cancers, is known to cause serious nephrotoxicity among certain populations.[12] In general, cisplatin can preferentially accumulate in renal tubular cells and induce mitochondrial dysfunction due to the increase of endogenous ROS level *via* depletion of GSH and inactivation of antioxidant enzymes,[12–14] which results in the induction of tubular epithelial cell damage.[15] Hence the superoxide anion radical ($O_2^{\bullet-}$), the precursor of most ROS,[16] can therefore act as an early symptom of nephrotoxicity for detecting and studying drug-induced AKI. Hence, the development of noninvasive detection of $O_2^{\bullet-}$ in mitochondria would be an efficient way to evaluate and predict drug-induced AKI.

Fluorescence imaging techniques, as a noninvasive tool, create enormous possibilities and provide new opportunities for the detection of small-molecules and real-time evaluation of cellular damage in preclinical studies.[17–23] Fluorescent probes

[a]State Key Laboratory of Chemo/Biosensing and Chemometrics, College of Chemistry and Chemical Engineering, Hunan University, Changsha, 410082, PR China. E-mail: lyuan@hnu.edu.cn

[b]Lab of Biosystem and Microanalysis, State Key Laboratory of Bioreactor Engineering, East China University of Science and Technology, Shanghai, 200237, China

[c]Laboratory of Bioimaging Probe Development, Singapore Bioimaging Consortium, Agency for Science, Technology and Research (A*STAR), 11 Biopolis Way, Helios #02-02, 138667, Singapore

[d]College of Materials Science and Engineering, Hunan University, Changsha 410082, PR China

† Electronic supplementary information (ESI) available: Experimental procedures, characterization data, and additional spectra. See DOI: 10.1039/c8sc03308k

‡ These authors contributed equally to this work.

with two-photon (TP) excitation or near-infrared (NIR) emission (650–900 nm) are more attractive because of weak specimen photodamage, low background fluorescence and deep tissue penetration in living systems.[24,25] At present, some TP or NIR fluorescent probes have been developed for the detection of $O_2^{\bullet-}$ in biological systems.[26–32] However, desirable TP or NIR fluorescent probes with high selectivity and sensitivity for investigating the role of $O_2^{\bullet-}$ in drug-induced nephrotoxicity are still lacking.

In this work, we reported two mitochondria-targeted fluorescent probes, one two-photon fluorescent probe (**Naph-$O_2^{\bullet-}$**) and one NIR fluorescent probe (**NIR-$O_2^{\bullet-}$**) for investigating AKI through mapping the fluctuation of $O_2^{\bullet-}$ by the combination of rational design and a screening approach. These probes showed excellent sensitivity and high selectivity toward $O_2^{\bullet-}$ in physiological environments without interference from other species. Moreover, these probes were successfully applied for imaging of endogenous $O_2^{\bullet-}$ in living cells and tissues and visualizing the small fluctuation of the $O_2^{\bullet-}$ level in drug-induced pathological nephrotoxicity for the first time.

Results and discussion

Screening and design of probes

Up to now, many small molecule fluorescent probes for $O_2^{\bullet-}$ have been reported by utilizing the oxidizability and nucleophilicity of $O_2^{\bullet-}$.[33–40] And some of these probes that are based on a nucleophilic reaction mechanism possess high sensitivity toward $O_2^{\bullet-}$. However, distinguishable detection of $O_2^{\bullet-}$ remains a big challenge due to the disturbance from other biological species with similar properties, such as H_2O_2 and GSH, especially in a multiple species coexisting physiological context.[41,42] To address this issue, we prepared a series of compounds as candidate probes and examined the response of these probes to $O_2^{\bullet-}$ by a screening method. Inspired by previous studies, the protection–deprotection strategy of hydroxyl groups on fluorophores is employed for $O_2^{\bullet-}$ sensing, such as $O_2^{\bullet-}$-induced deprotection of trifluoromethanesulfonate,[43] 2,4-dinitrobenzenesulfonyl[36,38] or diphenyl phosphinated[39,40] groups. In general, the protection of the hydroxyl group of fluorophores weakens their π-conjugation, leading to the weak fluorescence of caged fluorophores. Whereas, upon reaction with $O_2^{\bullet-}$, the uncaged fluorophores will recover their fluorescence, resulting in an "off–on" fluorescence response toward $O_2^{\bullet-}$ (Scheme 1A). The hydroxyl naphthalimide chromophore was selected as a signal platform due to its high fluorescence quantum yield, outstanding photostability and excellent two-photon properties.[44] Accordingly, some potential protective groups were introduced into the hydroxyl group of chromophores as the reaction site of $O_2^{\bullet-}$, including trifluoromethanesulfonate, 2,4-dinitrobenzenesulfonyl, 4-nitrobenzenesulfonyl, and diphenyl phosphinated, to afford compounds **1–4** (Scheme 1B).

With compounds **1–4** in hand, we first evaluated the reactivity of these probes towards $O_2^{\bullet-}$ under physiological conditions. As shown in Fig. S1,† compounds **2** and **3** displayed minor fluorescence enhancement after addition of $O_2^{\bullet-}$, while compound **1** exhibited a significantly substantial fluorescence increase. These results indicate that compound **1** is more

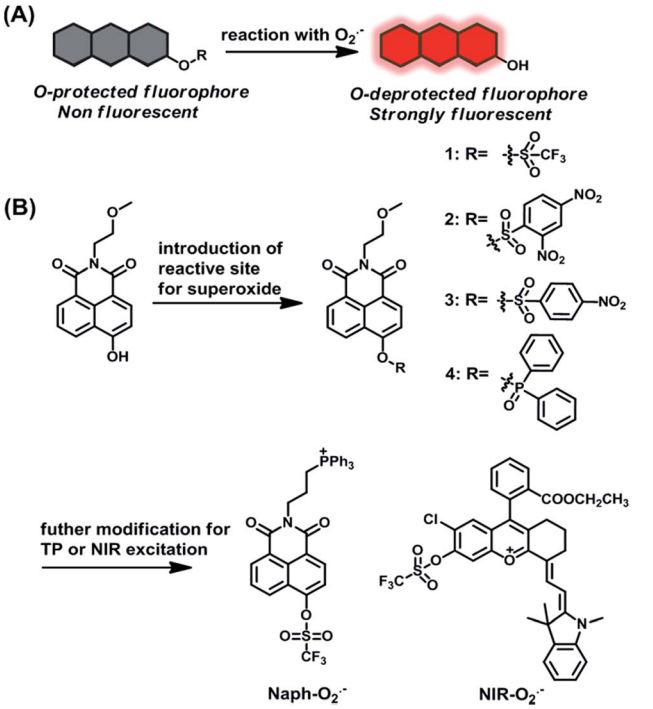

Scheme 1 (A) The strategy of designing hydroxyl protection/deprotection-based fluorescent $O_2^{\bullet-}$ probes. (B) Design of a series of compounds for sensing $O_2^{\bullet-}$ and the structures of the proposed mitochondria-targeted fluorescent probes for $O_2^{\bullet-}$.

sensitive to $O_2^{\bullet-}$ than compounds **2** and **3**. We then further investigated the selectivity of compounds **1–3** to various oxidant/nucleophilic species. As shown in Fig. S2,† compound **1** showed excellent selectivity for $O_2^{\bullet-}$, whereas, compound **2** and **3** were susceptible by other related biological agents (*e.g.* GSH and H_2S_2). Compared with **1**, compound **4** also showed relatively good sensitivity and high selectivity toward $O_2^{\bullet-}$ (Fig. S1 and S2†); however, compound **4** itself is relatively unstable in PBS solution, as shown in Fig. S3.† Therefore, the above results revealed that the trifluoromethyl group is a competent candidate reaction site for $O_2^{\bullet-}$ with high sensitivity and selectivity. To obtain the mitochondria targeting ability, the hydroxylnaphthalimide chromophore was further modified with a triphenylphosphine (TPP)[45,46] group to construct mitochondria-targeted probe **Naph-$O_2^{\bullet-}$** with two-photon excitation potential. Furthermore, to investigate mitochondrial $O_2^{\bullet-}$ at different tissues and *in vivo* levels in a drug-induced nephrotoxicity model, a NIR probe **NIR-$O_2^{\bullet-}$** was also constructed based on a positively charged merocyanine NIR dye[47,48] through simple chemical synthesis (Scheme 1B) (for synthetic and characterization details, see the ESI†).

Spectral response of the probes to $O_2^{\bullet-}$

The capability of probes to respond to $O_2^{\bullet-}$ was evaluated at room temperature. Before that, the stability of **NIR-$O_2^{\bullet-}$** and **Naph-$O_2^{\bullet-}$** was first measured (Fig. S4†), showing that they were latent for $O_2^{\bullet-}$ recognition. As shown in Fig. 1A, **NIR-$O_2^{\bullet-}$** shows feeble fluorescence (Φ < 0.01) in the absence of $O_2^{\bullet-}$. Upon

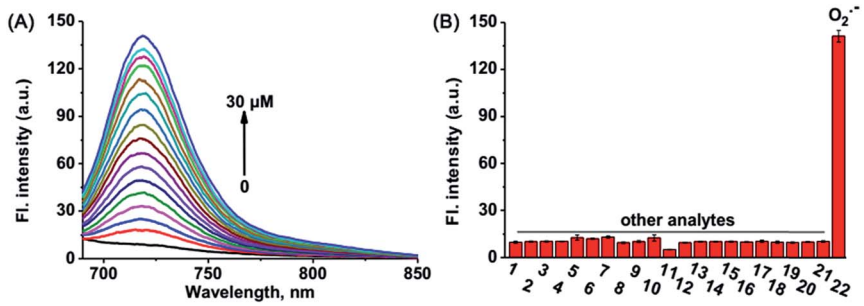

Fig. 1 Fluorescence spectra of (A) **NIR-$O_2^{\bullet-}$** (5 μM) in PBS buffer solution (25 mM, 20% CH_3CN, pH 7.4) upon addition of $O_2^{\bullet-}$ (0–30 μM). (B) Fluorescence intensity of **NIR-$O_2^{\bullet-}$** (5 μM) in PBS buffer solution (25 mM, 20% CH_3CN, pH 7.4) toward $O_2^{\bullet-}$ (30 μM) and other analytes: (1) blank; (2) Ca^{2+} (100 μM); (3) CH_3COO^- (100 μM); (4) Cu^{2+} (100 μM); (5) Cys (100 μM); (6) Fe^{3+} (100 μM); (7) GSH (1 mM); (8) H_2O_2 (100 μM); (9) H_2S (100 μM); (10) H_2S_2 (50 μM); (11) HOCl (100 μM); (12) HSO_3^- (100 μM); (13) K^+ (100 μM); (14) Mg^{2+} (100 μM); (15) Na^+ (100 μM); (16) NO (100 μM); (17) NO_2^- (100 μM); (18) SIN-1 (25 μM); (19) SO_3^{2-} (100 μM); (20) SO_4^{2-} (100 μM); (21) Zn^{2+} (100 μM); (22) $O_2^{\bullet-}$. The mixture was kept for 30 min at room temperature before the fluorescence intensity of the probe solution was recorded. The excitation wavelength was 660 nm.

incubation with various concentrations (0–30 μM) of $O_2^{\bullet-}$, the fluorescence intensity (with a maximum at 719 nm) increased with the increase of $O_2^{\bullet-}$ concentration ($\Phi = 0.55$). In addition, the fluorescence intensity showed an excellent linear relationship ($R^2 = 0.999$) in the concentration range of 0–5 μM $O_2^{\bullet-}$ (Fig. S5†), and a detection limit of 0.24 μM was calculated (S/N = 3), which was significantly lower than that of $O_2^{\bullet-}$ in healthy individuals.[49] And the maximum absorption of **NIR-$O_2^{\bullet-}$** centered at 548/576 nm gradually decreased, while a new absorption peak at 698 nm appeared after addition of $O_2^{\bullet-}$ (Fig. S6†). These results imply that probe **NIR-$O_2^{\bullet-}$** displays superior sensitivity to $O_2^{\bullet-}$ and has the capability to monitor trace amounts of intracellular $O_2^{\bullet-}$ in AKI *in vivo*. Additionally, the spectral response of **Naph-$O_2^{\bullet-}$** to $O_2^{\bullet-}$ was also examined. As shown in Fig. S7,† **Naph-$O_2^{\bullet-}$** ($\Phi = 0.008$) showed a dramatic fluorescence enhancement ($\Phi = 0.51$) of more than 25-fold centered at 554 nm upon the addition of $O_2^{\bullet-}$. The fluorescence intensity at 554 nm reaches a plateau when the amount of $O_2^{\bullet-}$ is greater than 50 μM (Fig. S8†). The detection limit was calculated to be 0.39 μM (Fig. S9†), the high sensitivity of **Naph-$O_2^{\bullet-}$** ensures its application in detecting endogenous $O_2^{\bullet-}$ in biological systems.

To simulate the physiological mitochondrial environment, spectra fluorometric titrations of probes **NIR-$O_2^{\bullet-}$** and **Naph-$O_2^{\bullet-}$** were performed in buffer solution at pH = 7.8. The results showed a more notable change with the increase in the dose of $O_2^{\bullet-}$ (Fig. S10 and S11†). Then the fluorescence response of **NIR-$O_2^{\bullet-}$** and **Naph-$O_2^{\bullet-}$** to $O_2^{\bullet-}$ was also evaluated at different pH values. As shown in Fig. S12 and S13,† the fluorescence intensity of **NIR-$O_2^{\bullet-}$** and **Naph-$O_2^{\bullet-}$** is stable over the range of pH 6.0 to 8.5, while obvious fluorescence enhancement is observed upon addition of $O_2^{\bullet-}$ in the range of mitochondria-relevant pH from 7.0 to 8.5. In addition, the fluorescence intensity of **NIR-OH** and **Naph-OH** did not change when pH > 6.5 (Fig. S14 and S15†). The above results indicate that **NIR-$O_2^{\bullet-}$** and **Naph-$O_2^{\bullet-}$** have potential applications for the detection of mitochondrial $O_2^{\bullet-}$.

The selectivity of the probes was evaluated in detail by testing the fluorescence changes after exposure to panels of ROS, RNS, RSS and other relevant biological analytes. As shown in Fig. 1B and S16,† a striking enhancement of fluorescence intensity is triggered only by $O_2^{\bullet-}$, and there is no obvious change in the fluorescence intensity when adding other ROS, RNS, RSS (H_2O_2, $O_2^{\bullet-}$, NO, $ONOO^-$, HOCl, H_2S, H_2S_2, HSO_3^-, SO_3^{2-}, Cys, and GSH), and biorelevant anions and cations (NO_2^-, SO_4^{2-}, CH_3COO^-, Na^+, K^+, Mg^{2+}, Fe^{2+}, and Cu^{2+}). These results collectively demonstrated the excellent selectivity of probes **NIR-$O_2^{\bullet-}$** and **Naph-$O_2^{\bullet-}$** toward $O_2^{\bullet-}$.

Proposed mechanism

According to previous reports,[43] $O_2^{\bullet-}$ might induce the release of a trifluoromethyl group from the hydroxyl group on the fluorophores *via* a nucleophilic addition reaction, and finally yield a hydroxyl-deprotected product (Scheme S2†). To verify this hypothesis, the reaction mixture of **Naph-$O_2^{\bullet-}$**/**NIR-$O_2^{\bullet-}$** and $O_2^{\bullet-}$ was analyzed by mass spectrometry. The peaks of two products with m/z = 515.2 and m/z = 565.1 were observed, respectively (Fig. S17 and S18†). Furthermore, high-performance liquid chromatography (HPLC) analysis also confirmed the reaction mechanism of **NIR-$O_2^{\bullet-}$** and **Naph-$O_2^{\bullet-}$** with $O_2^{\bullet-}$ (Fig. S19 and S20†). The probe **NIR-$O_2^{\bullet-}$** (or **Naph-$O_2^{\bullet-}$**) only gives a single peak at 22.1 min (or 19.5 min); however, the proposed product 7 (or **Naph-OH**) shows a single peak at 13.3 min (or 8.5 min). Upon the addition of $O_2^{\bullet-}$ to the probe solution for 30 min, a peak corresponding to the compound 7 (or **Naph-OH**) appeared at 13.3 min (or 8.5 min) and the peak of the probe at 22.1 min (or 19.5 min) decreased in the meantime. Therefore, the results are in good agreement with the proposed mechanism (Scheme S2†).

Fluorescence imaging of $O_2^{\bullet-}$ in living cells

Then, we examined the potential of **Naph-$O_2^{\bullet-}$** and **NIR-$O_2^{\bullet-}$** for monitoring endogenous $O_2^{\bullet-}$ in living cells by two/one-photon microscopy imaging. In order to avoid underlying interference caused by other biological oxidants and nucleophilic reagents, the selectivity assay of probes to detect $O_2^{\bullet-}$ was further carried out in cells. H_2O_2 and SO_3^{2-} were selected as the representative

interfering oxidants and nucleophilic reagents in this experiment. As shown in Fig. 2A and B, HepG2 cells incubated with free probes **Naph-$O_2^{\bullet-}$** or **NIR-$O_2^{\bullet-}$** showed negligible fluorescence in the green channel or in the red channel. However, a dramatic enhancement of fluorescence could be observed when the cells were pretreated with LPS/IFN-γ before incubation with probes **Naph-$O_2^{\bullet-}$** or **NIR-$O_2^{\bullet-}$**. In contrast, the cells displayed minor fluorescence enhancement in both channels when pretreated with H_2O_2 or SO_3^{2-} before incubation with probes, which meant that the probes were especially capable of monitoring endogenous $O_2^{\bullet-}$ and had little interference in living cells. Moreover, the cells were first incubated with 2,2,6,6-tetramethylpiperidine-*N*-oxyl (TEMPO)[50] and tiron,[26] before the addition of probes as negative control groups. However, there was no obvious fluorescence increase observed for the LPS/IFN-γ-pretreated HepG2 cells when stimulated with TEMPO or titron. The main reason probably comes from the scavenging effect of TEMPO and titron on cellular $O_2^{\bullet-}$ production. It is worth noting that in HepG2 and HeLa cells, **Naph-$O_2^{\bullet-}$** can also be used for $O_2^{\bullet-}$ imaging by confocal fluorescence microscopy (Fig. S21 and S22†). In addition, these probes exhibited low cytotoxicity to live HepG2 cells when evaluated by MTT assays (Fig. S23†). Taken together, these results demonstrated that **Naph-$O_2^{\bullet-}$** and **NIR-$O_2^{\bullet-}$** show great potential for specific imaging of endogenously produced $O_2^{\bullet-}$ in living cells.

To confirm the target specificity of **NIR-$O_2^{\bullet-}$** at a subcellular level, colocalization experiments were performed in HepG2 cells using the commercial fluorescent probes Mito-Tracker Green and Lyso-Tracker Red. The cells were pre-treated with LPS/IFN-γ for 12 h and subsequently treated with Mito-Tracker Green or Lyso-Tracker Red (1 μM) for another 10 min. As shown in Fig. 3, the fluorescence of **NIR-$O_2^{\bullet-}$** in the red channel overlapped well with that of Mito-Tracker Green (Pearson's correlation coefficient: 0.92). In contrast, a poor overlap between the fluorescence of probe**NIR-$O_2^{\bullet-}$** and Lyso-Tracker Red was observed (Pearson's correlation coefficient: 0.54). We also confirmed that **NIR-$O_2^{\bullet-}$** can target mitochondria in HK-2 cells (Fig. S24†). Similar results were found in the case of **Naph-$O_2^{\bullet-}$** (Pearson's correlation coefficient: 0.91) (Fig. S25†). Thus, both probes **NIR-$O_2^{\bullet-}$** and **Naph-$O_2^{\bullet-}$** are latent tools for distinguished imaging of mitochondrial $O_2^{\bullet-}$.

Fluorescence imaging of $O_2^{\bullet-}$ in drug-induced nephrotoxicity in living HK-2 cells

Encouraged by the results described above, we then examined the potential use of **NIR-$O_2^{\bullet-}$** and **Naph-$O_2^{\bullet-}$** to visualize $O_2^{\bullet-}$ in cisplatin-induced living kidney cells, a commercially available drug antitumor, which is known to trigger acute kidney damage.[12] The protective effect of antioxidants against cisplatin-induced oxidative stress would occur in experimental nephrotoxicity,[51,52] such as L-carnitine (LC), an L-lysine derivative. We observed that human kidney 2 (HK-2) cells only display feeble fluorescence when incubated with **NIR-$O_2^{\bullet-}$** for 30 min (Fig. 4a). In contrast, HK-2 cells gave bright fluorescence and dose-dependent enhancement when the cells were pre-incubated with different concentrations of cisplatin (100–1000 μM) for 12 h and then treated with **NIR-$O_2^{\bullet-}$** for another 30 min (Fig. 4a–e). A 3.7-fold fluorescence enhancement was observed after incubation with 1000 μM cisplatin (Fig. 4j). However, the fluorescence is significantly reduced (Fig. 4f–j) in a dose-dependent way by the pretreatment with L-carnitine (LC), a known antioxidant that could against cisplatin-induced oxidative stress in experimental nephrotoxicity.[53] Moreover, a similar fluorescence change could be observed by using probe **Naph-$O_2^{\bullet-}$** in a two-photon model in HK-2 cells in cisplatin-induced nephrotoxicity (Fig. S26†). In short, these observations indicate that **NIR-$O_2^{\bullet-}$** and **Naph-$O_2^{\bullet-}$** are promising

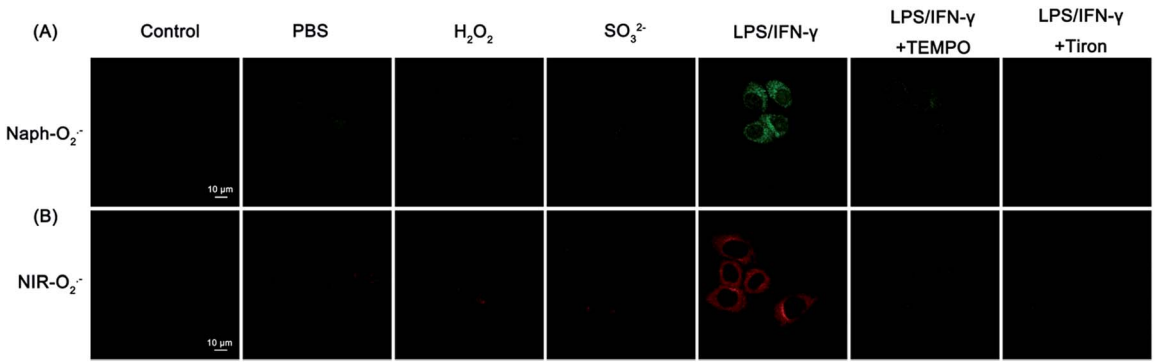

Fig. 2 Pseudo-color fluorescence images of probes **Naph-$O_2^{\bullet-}$** and **NIR-$O_2^{\bullet-}$** in HepG2 cells under different conditions by two-photon (A) or one-photon (B) confocal fluorescence imaging. First column: the fluorescence images of intact HepG2 cells. Second column: cells were incubated with probe **Naph-$O_2^{\bullet-}$** (5 μM, 30 min)/**NIR-$O_2^{\bullet-}$** (5 μM, 30 min) and then imaged. Third and fourth columns: cells were pretreated with probe **Naph-$O_2^{\bullet-}$** (5 μM, 30 min)/**NIR-$O_2^{\bullet-}$** (5 μM, 30 min), subsequently incubated with H_2O_2 (100 μM) (third column) or SO_3^{2-} (100 μM) (fourth column) for 30 min, and then imaged. Fifth column: cells were prestimulated with LPS (1 μg mL^{-1}) and IFN-γ (50 ng mL^{-1}) for 12 h, subsequently incubated with probe **Naph-$O_2^{\bullet-}$** (5 μM, 30 min) or **NIR-$O_2^{\bullet-}$** (5 μM, 30 min), and then imaged. Sixth and seventh columns: cells were pretreated with $O_2^{\bullet-}$ scavenger TEMPO (300 μM) (sixth column) or tiron (10 μM) (seventh column) during stimulation with LPS (1 μg mL^{-1}) and IFN-γ (50 ng mL^{-1}) for 12 h, subsequently incubated with probe **Naph-$O_2^{\bullet-}$** (5 μM, 30 min) or **NIR-$O_2^{\bullet-}$** (5 μM, 30 min), and then imaged. The fluorescence images were captured from the green channel of 500–550 nm and 663–738 nm with excitation at 800 and 640 nm, respectively. Scale bar: 10 μm.

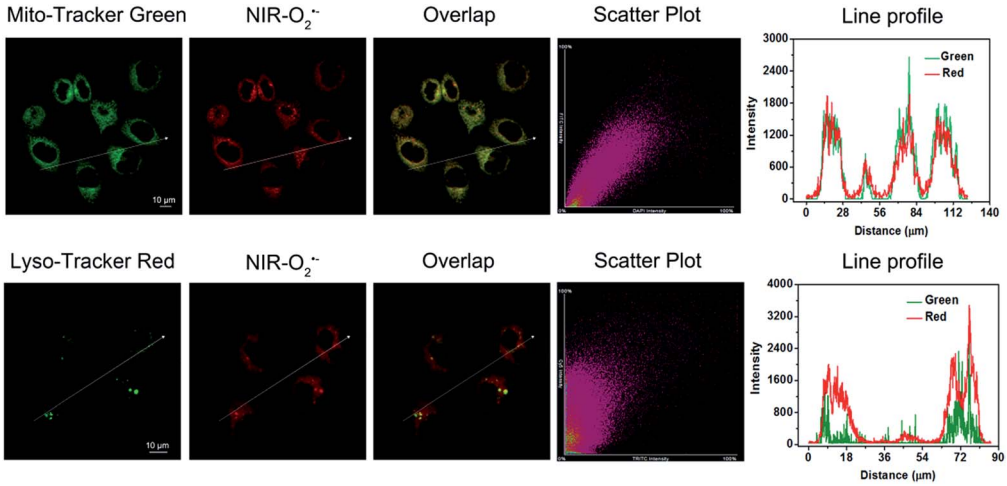

Fig. 3 Intracellular localization of **NIR-$O_2^{\bullet-}$** in HepG2 cells. Images of HepG2 cells pre-treated with LPS (1 μg mL^{-1}) and IFN-γ (50 ng mL^{-1}) for 12 h, then incubated with 5 μM **NIR-$O_2^{\bullet-}$** for 30 min and subsequently added 1 μM Mito-Tracker Green (or 1 μM Lyso-Tracker Red) for 10 min. First column: green channel of Mito-Tracker Green (λ_{ex} = 488 nm, λ_{em} = 500–550 nm) and Lyso-Tracker Red fluorescence (λ_{ex} = 561 nm, λ_{em} = 570–620 nm); second column: red channel of the probe (λ_{ex} = 640 nm, λ_{em} = 663–738 nm); third column: merged signal. Scatter plot: the overlap of green and red channel images. Line profile: intensity profile of the white line in image overlap. Scale bar: 10 μm.

probes for the detection of endogenous $O_2^{\bullet-}$ in live cells. In addition, the increase of $O_2^{\bullet-}$ level is closely related to the drug induced AKI process in living HK-2 cells.

Living kidney tissues imaging of $O_2^{\bullet-}$ in drug-induced nephrotoxicity

Next, the capability of probes for monitoring $O_2^{\bullet-}$ in live tissues was evaluated in a drug-induced AKI mouse model. BALB/c mice were first intraperitoneally injected with cisplatin (20 mg kg^{-1}) to generate an AKI model and PBS was used as the control group. After 48 h, the mice were sacrificed and the kidneys were sectioned for tissue fluorescence imaging. The kidney slices were treated with probe **Naph-$O_2^{\bullet-}$** (10 μM) or **NIR-$O_2^{\bullet-}$** (5 μM) for 30 min. As shown in Fig. 5, compared to the control group, the kidney tissues from cisplatin-induced AKI mice exhibited a distinctly enhanced fluorescence in the green or red channel, which indicated that probes **Naph-$O_2^{\bullet-}$** and **NIR-$O_2^{\bullet-}$** are efficient in evaluating cisplatin-induced AKI. Moreover, the fluorescence signal changes can be detected in

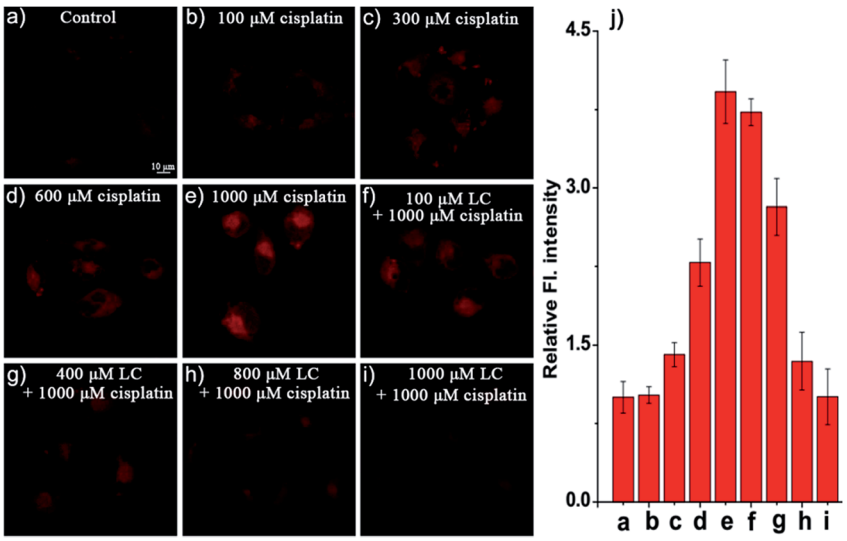

Fig. 4 Fluorescence images of $O_2^{\bullet-}$ in drug-induced nephrotoxicity in HK-2 cells. Images were obtained with the addition of 5 μM **NIR-$O_2^{\bullet-}$** in the same confocal dish (a–i). (a) The HK-2 cells were treated with 5 μM **NIR-$O_2^{\bullet-}$**; (b–e) cells were pre-treated with different concentrations of cisplatin (100 μM, 300 μM, 600 μM, and 1000 μM) for 12 h, and then treated with 5 μM probe **NIR-$O_2^{\bullet-}$** for 30 min; (f–i) cells were pre-incubated with different concentrations of LC (100 μM, 400 μM, 800 μM, and 1000 μM) in the presence of cisplatin (1000 μM) for 12 h, and then treated with 5 μM probe **NIR-$O_2^{\bullet-}$** for 30 min. (j) Average intensity in (a–i), respectively. Data are expressed as mean ± SD of three parallel experiments. The excitation wavelength was 640 nm. The emission band was at 663–738 nm. Scale bar = 10 μm.

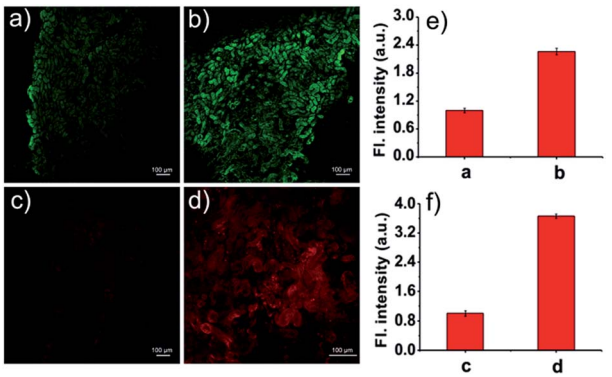

Fig. 5 Fluorescence images of a fresh rat kidney slice with a magnification of 10× by two-photon (a and b) and one photon (c and d) confocal imaging. PBS (320 μL) and cisplatin (320 μL, 20 mg kg^{-1}) were subcutaneously injected into the abdominal cavity of mice to be the control group (a and c) and to cause acute kidney injury (b and d), respectively. After 48 h, the kidney was dissected and then incubated with **Naph-$O_2^{\bullet-}$** (10 μM, a and b) and **NIR-$O_2^{\bullet-}$** (5 μM, c and d) for 30 min. (e and f) Average fluorescence intensity in panels (a–d). Excitation at 800 nm (two-photon laser, a and b) and 640 nm (one-photon laser, c and d). Emission bands were at 500–550 nm in the green channel and 663–738 nm in the red channel. Scale bar: 100 μm.

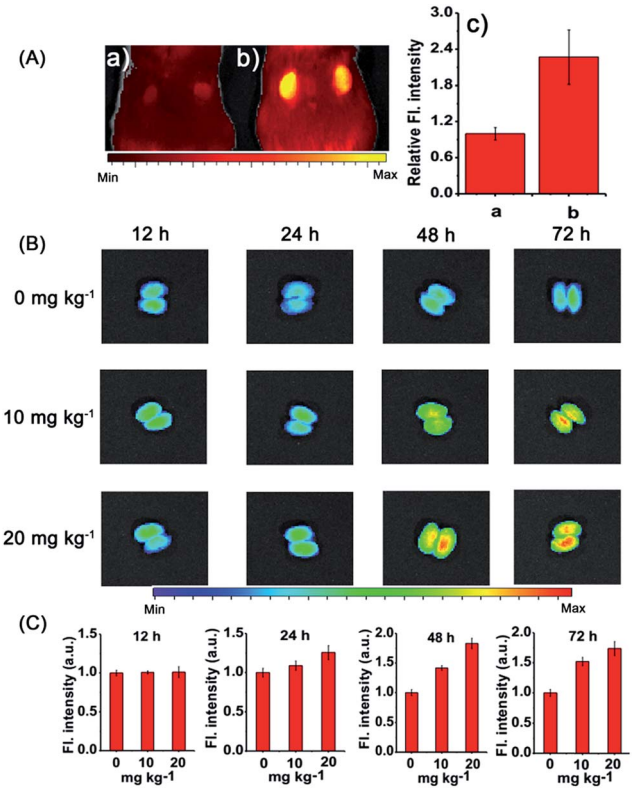

Fig. 6 (A) *In vivo* fluorescence imaging of mice that were intraperitoneally pre-injected with (a) PBS and (b) 20 mg kg^{-1} cisplatin before intravenous injection of **NIR-$O_2^{\bullet-}$** (100 μL × 200 μM) in PBS. (c) Average fluorescence intensity in (a and b). (B) Fluorescence images of the kidney of a series of mice injected intraperitoneally with cisplatin of varied concentrations (0, 10, and 20 mg kg^{-1}) for different time periods (12, 24, 48, and 72 h) and then intravenously injected with the **NIR-$O_2^{\bullet-}$** (100 μL × 100 μM). (C) Average fluorescence intensity for images in (B). Values are the mean ± SD for $n = 4$.

kidney tissue-incubated **Naph-$O_2^{\bullet-}$** at a depth of 130 μm in the two-photon mode (Fig. S27†). The imaging depth can be detected to be 50 μm deeper than that in the one-photon mode (Fig. S28†). The changes of the detectable fluorescence signal were also observed in AKI kidney tissues within 110 μm by using probe **NIR-$O_2^{\bullet-}$** (Fig. S29†). In summary, these results demonstrated that both **Naph-$O_2^{\bullet-}$** and **NIR-$O_2^{\bullet-}$** are capable of visualization of $O_2^{\bullet-}$ in living kidney tissues by using two/one photon fluorescence imaging, further showing their capability in renal injury studies.

Fluorescence imaging of $O_2^{\bullet-}$ in drug-induced nephrotoxicity *in vivo*

Afterwards, we applied probe **NIR-$O_2^{\bullet-}$** to trace the endogenous $O_2^{\bullet-}$ level *in vivo*, which is due to drug-induced AKI. As shown in Fig. 6A, the cisplatin treated intact mice exhibited a substantial enhancement of fluorescence, indicating an increased level of $O_2^{\bullet-}$ in AKI. Interestingly, increased fluorescence signals in the liver region were observed in cisplatin-treated mice (Fig. S30†). We proposed that this may be due to other side effects of cisplatin, which can lead to liver injury to a less serious extent.[54] To further verify the possibility of monitoring cisplatin-induced nephrotoxicity *in vivo* by using **NIR-$O_2^{\bullet-}$**, intraperitoneal injection of cisplatin in dose-dependent (0, 10 and 20 mg kg^{-1}) and time-dependent (12, 24, 48 and 72 h) manners were carried out, and then the probe (100 μL of 100 μM stock solution) was injected through the tail vein of the mice. After 45 min, the kidneys were harvested from the mice for fluorescence imaging. As shown in Fig. 6B, the images captured from the cisplatin-stimulated mice exhibited remarkable enhancement of signals in the kidney, while no change of fluorescence intensity was observed for the control samples that were only treated with the probe. The results indicated that the cisplatin could cause severe acute kidney injury at a 20 mg kg^{-1} dose and 48 h treatment time (Fig. 6C). Consequently, it is conceivable that **NIR-$O_2^{\bullet-}$** is appropriate for evaluating cisplatin-induced nephrotoxicity in response to oxidative stress.

Finally, probe **NIR-$O_2^{\bullet-}$** was employed to evaluate cisplatin-induced nephrotoxicity and L-carnitine (LC) remediation *in vivo* (Fig. 7A). The experiment was divided into three groups. One group was injected with PBS (320 μL) in the peritoneal cavity, followed by intravenous injection with **NIR-$O_2^{\bullet-}$** (100 μL, 100 μM) as the negative control group; the second group was intraperitoneally injected with cisplatin (320 μL, 20 mg kg^{-1}), followed by intravenous injection with the probe **NIR-$O_2^{\bullet-}$** (100 μL, 100 μM) 48 h later; while the third group was intraperitoneally injected with LC (60 μL, 400 mg kg^{-1}) 48 h before cisplatin (320 μL, 20 mg kg^{-1}), followed by intravenous injection with the probe **NIR-$O_2^{\bullet-}$** (100 μL, 100 μM). As shown in Fig. 7A, the kidney of the mice pretreated with cisplatin exhibited a distinct fluorescence increase (Fig. 7A(e)) compared to the control group (Fig. 7A(d)). Excitingly, the fluorescence of the LC pretreatment group was dramatically suppressed compared with that of the group without LC, which should be

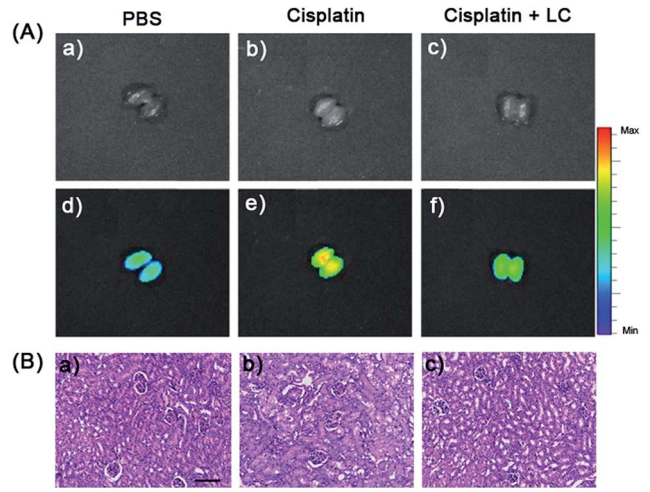

Fig. 7 (A) Fluorescence images of the kidney in nephrotoxicity using NIR-$O_2^{\bullet-}$. The mice were injected intraperitoneally with (a and d) PBS (320 μL) or (b and e) cisplatin (320 μL, 20 mg kg^{-1}) for 48 h, or (c and f) LC (60 μL, 400 mg kg^{-1}) for 48 h and cisplatin (320 μL, 20 mg kg^{-1}) for 48 h in succession, then intravenous injected with the NIR-$O_2^{\bullet-}$ (100 μL, 100 μM) for 45 min, and subsequently the kidney was dissected for imaging. Excitation at 640 nm. Emission channel at 695–770 nm. (B) Representative H&E staining images of the kidney of mice in panel (A). Scale bar: 100 μm.

ascribed to the alleviation of the kidney injury caused by the drug LC (Fig. 7A(f)). It is worth noting that a similar phenomenon can be observed in the liver with a smaller variation degree of fluorescence (Fig. S31†), which may be a slight liver injury caused by the side effects of drug cisplatin.[54] In addition, the protective effect of LC was also identified by hematoxylin–eosin (H&E) staining. Compared with the cisplatin treated kidney, the proportion of injured kidney tissues is much smaller when pretreated with LC (Fig. 7B). The results indicated that LC could reduce the injury caused by cisplatin to the kidney, which was consistent with fluorescence imaging (Fig. 7A). To the best of our knowledge, **NIR-$O_2^{\bullet-}$** is the first NIR fluorescent probe for the imaging of $O_2^{\bullet-}$ in drug induced nephrotoxicity.

Conclusions

In summary, we have constructed a two-photon fluorescent probe **Naph-$O_2^{\bullet-}$** and a NIR fluorescent probe **NIR-$O_2^{\bullet-}$** with mitochondria-targeting ability by probe-screening strategies, which are used for highly selective monitoring of $O_2^{\bullet-}$ *in vitro* and *in vivo*. The utility of these reaction-based probes for $O_2^{\bullet-}$ detection has been fully verified in terms of their excellent sensitivity and selectivity to various biological oxidants and nucleophilic reagents. Moreover, the excellent performance in cell and tissue imaging illustrated that probes **Naph-$O_2^{\bullet-}$** and **NIR-$O_2^{\bullet-}$** could be used to monitor endogenous $O_2^{\bullet-}$ by two-photon or one-photon fluorescence confocal microscopy. Furthermore, probe **NIR-$O_2^{\bullet-}$** was further demonstrated to be able to visualize the cisplatin-induced acute kidney injury and LC remediation related to $O_2^{\bullet-}$ levels *in vivo* for the first time. We anticipate that these probes can serve as promising fluorescent tools for facilitate biomedical study on the roles of $O_2^{\bullet-}$ in various kidney injury diseases.

Conflicts of interest

There are no conflicts to declare.

Acknowledgements

This work was financially supported by the NSFC (21622504, 21735001, and 21877029), the Science and Technology Project of Hunan Province (2017RS3019), and the Open Funding Project of the State Key Laboratory of Bioreactor Engineering. All animal procedures were performed in accordance with the Guidelines for Care and Use of Laboratory Animals of Hunan University and experiments were approved by the Animal Ethics Committee of College of Biology (Hunan University).

Notes and references

1 K. Hosohata, *Int. J. Mol. Sci.*, 2016, **17**, 1826–1836.
2 K. I. Inui, S. Masuda and H. Saito, *Kidney Int.*, 2000, **58**, 944–958.
3 H. Izzedine and M. A. Perazella, *Kidney International Reports*, 2017, **2**, 504–514.
4 R. D. Beger, J. Sun and L. K. Schnackenberg, *Toxicol. Appl. Pharmacol.*, 2010, **243**, 154–166.
5 G. Benedetti, B. van de Water and M. de Graauw, *Toxicogenomics-Based Cellular Models*, Academic Press, 2014.
6 D. Sasaki, A. Yamada, H. Umeno, H. Kurihara, S. Nakatsuji, S. Fujihira, K. Tsubota, M. Ono, A. Moriguchi, K. Watanabe and J. Seki, *Biomarkers*, 2011, **16**, 553–566.
7 P. Espandiari, J. Zhang, B. A. Rosenzweig, V. S. Vaidya, J. Sun, L. Schnackenberg, E. H. Herman, A. Knapton, J. V. Bonventre, R. D. Beger, K. L. Thompson and J. Hanig, *Toxicol. Sci.*, 2007, **99**, 637–648.
8 Y. Zhou, V. S. Vaidya, R. P. Brown, J. Zhang, B. A. Rosenzweig, K. L. Thompson, T. J. Miller, J. V. Bonventre and P. L. Goering, *Toxicol. Sci.*, 2008, **101**, 159–170.
9 C. Gluhovschi, G. Gluhovschi, L. Petrica, R. Timar, S. Velciov, I. Ionita, A. Kaycsa and B. Timar, *J. Diabetes Res.*, 2016, **2016**, 4626125–4626137.
10 R. P. Miller, R. K. Tadagavadi, G. Ramesh and W. B. Reeves, *Toxins*, 2010, **2**, 2490–2518.
11 N. A. Santos, C. S. Catao, N. M. Martins, C. Curti, M. L. Bianchi and A. C. Santos, *Arch. Toxicol.*, 2007, **81**, 495–504.
12 R. W. Schrier, *J. Clin. Invest.*, 2002, **110**, 743–745.
13 İ. Durak, H. Özbek, M. Karaayvaz and H. S. Öztürk, *Drug and Chemical Toxicology*, 2002, **25**, 1–8.
14 R. Baliga, N. Ueda, P. D. Walker and S. V. Shah, *Am. J. Kidney Dis.*, 1997, **29**, 465–477.
15 B. H. Ali, M. S. Al Moundhri, M. Tag Eldin, A. Nemmar and M. O. Tanira, *Fundam. Clin. Pharmacol.*, 2007, **21**, 547–553.
16 B. C. Dickinson, V. S. Lin and C. J. Chang, *Nat. Protoc.*, 2013, **8**, 1249–1259.

17 W. Xu, Z. Zeng, J.-H. Jiang, Y.-T. Chang and L. Yuan, *Angew. Chem., Int. Ed.*, 2016, **55**, 13658–13699.
18 Y. Liu, K. Li, K.-X. Xie, L.-L. Li, K.-K. Yu, X. Wang and X.-Q. Yu, *Chem. Commun.*, 2016, **52**, 3430–3433.
19 H. Zhang, R. Liu, J. Liu, L. Li, P. Wang, S. Q. Yao, Z. Xu and H. Sun, *Chem. Sci.*, 2016, **7**, 256–260.
20 X. Chen, T. Pradhan, F. Wang, J. S. Kim and J. Yoon, *Chem. Rev.*, 2012, **112**, 1910–1956.
21 H. Zhu, J. Fan, J. Du and X. Peng, *Acc. Chem. Res.*, 2016, **49**, 2115–2126.
22 M. Gao, R. Wang, F. Yu and L. Chen, *Biomaterials*, 2018, **160**, 1–14.
23 J. Zhang, X.-Y. Zhu, X.-X. Hu, H.-W. Liu, J. Li, L.-L. Feng, X. Yin, X.-B. Zhang and W. Tan, *Anal. Chem.*, 2016, **88**, 11892–11899.
24 F. Helmchen and W. Denk, *Nat. Methods*, 2005, **2**, 932–940.
25 X. Li, X. Gao, W. Shi and H. Ma, *Chem. Rev.*, 2014, **114**, 590–659.
26 X. Yang, Y. Zhou, X. Zhang, S. Yang, Y. Chen, J. Guo, X. Li, Z. Qing and R. Yang, *Chem. Commun.*, 2016, **52**, 10289–10292.
27 W. Zhang, X. Wang, P. Li, F. Huang, H. Wang, W. Zhang and B. Tang, *Chem. Commun.*, 2015, **51**, 9710–9713.
28 F. Yu, M. Gao, M. Li and L. Chen, *Biomaterials*, 2015, **63**, 93–101.
29 R. Liu, L. Zhang, Y. Chen, Z. Huang, Y. Huang and S. Zhao, *Anal. Chem.*, 2018, 4452–4460.
30 J. Zhang, C. Li, R. Zhang, F. Zhang, W. Liu, X. Liu, S. M. Lee and H. Zhang, *Chem. Commun.*, 2016, **52**, 2679–2682.
31 X. Han, R. Wang, X. Song, F. Yu, C. Lv and L. Chen, *Biomaterials*, 2018, **156**, 134–146.
32 R.-Q. Li, Z.-Q. Mao, L. Rong, N. Wu, Q. Lei, J.-Y. Zhu, L. Zhuang, X.-Z. Zhang and Z.-H. Liu, *Biosens. Bioelectron.*, 2017, **87**, 73–80.
33 S. Ma, W. Mu, J. Gao and J. Zhou, *J. Fluoresc.*, 2009, **19**, 487–493.
34 S. T. Manjare, S. Kim, W. D. Heo and D. G. Churchill, *Org. Lett.*, 2014, **16**, 410–412.
35 J. J. Gao, K. H. Xu, B. Tang, L. L. Yin, G. W. Yang and L. G. An, *FEBS J.*, 2007, **274**, 1725–1733.
36 F. Si, Y. Liu, K. Yan and W. Zhong, *Chem. Commun.*, 2015, **51**, 7931–7934.
37 H. K. D. P. Murale, W. S. Choi and D. G. Churchill, *Org. Lett.*, 2013, **15**, 3946–3949.
38 K. Y. H. Maeda, Y. Nomura, I. Kohno, L. Hafsi, N. Ueda, S. Yoshida, M. Fukuda, Y. Fukuyasu and Y. Yamauchi, *J. Am. Chem. Soc.*, 2005, **127**, 68–69.
39 K. Xu, X. Liu, B. Tang, G. Yang, Y. Yang and L. An, *Chem. –Eur. J.*, 2007, **13**, 1411–1416.
40 K. Xu, X. Liu and B. Tang, *ChemBioChem*, 2007, **8**, 453–458.
41 G. V. G. Rothe, *J. Leukocyte Biol.*, 1990, **47**, 440–448.
42 H. Maeda, H. Matsuno, M. Ushida, K. Katayama, K. Saeki and N. Itoh, *Angew. Chem., Int. Ed.*, 2005, **44**, 2922–2925.
43 J. J. Hu, N. K. Wong, S. Ye, X. Chen, M. Y. Lu, A. Q. Zhao, Y. Guo, A. C. Ma, A. Y. Leung, J. Shen and D. Yang, *J. Am. Chem. Soc.*, 2015, **137**, 6837–6843.
44 D. Cheng, W. Xu, L. Yuan and X. Zhang, *Anal. Chem.*, 2017, **89**, 7693–7700.
45 J. Zielonka, J. Joseph, A. Sikora, M. Hardy, O. Ouari, J. Vasquez-Vivar, G. Cheng, M. Lopez and B. Kalyanaraman, *Chem. Rev.*, 2017, **117**, 10043–10120.
46 Z. Xu and L. Xu, *Chem. Commun.*, 2016, **52**, 1094–1119.
47 Y. Wei, D. Cheng, T. Ren, Y. Li, Z. Zeng and L. Yuan, *Anal. Chem.*, 2016, **88**, 1842–1849.
48 X. Xiong, F. Song, G. Chen, W. Sun, J. Wang, P. Gao, Y. Zhang, B. Qiao, W. Li, S. Sun, J. Fan and X. Peng, *Chem. –Eur. J.*, 2013, **19**, 6538–6545.
49 C. C. Winterbourn, M. B. Hampton, J. H. Livesey and A. J. Kettle, *J. Biol. Chem.*, 2006, **281**, 39860–39869.
50 D. Cheng, Y. Pan, L. Wang, Z. Zeng, L. Yuan, X. Zhang and Y. T. Chang, *J. Am. Chem. Soc.*, 2017, **139**, 285–292.
51 C. A. Davis, H. S. Nick and A. Agarwal, *J. Am. Soc. Nephrol.*, 2001, **12**, 2683–2690.
52 A. Kuhad, N. Tirkey, S. Pilkhwal and K. Chopra, *BioFactors*, 2006, **26**, 1–12.
53 S. Zambrano, A. J. Blanca, M. V. Ruiz-Armenta, J. L. Miguel-Carrasco, M. Arevalo, A. Mate and C. M. Vazquez, *Am. J. Hypertens.*, 2014, **27**, 460–470.
54 M. A. Dkhil, S. Al-Quraishy, A. M. Aref, M. S. Othman, K. M. El-Deib and A. E. Abdel Moneim, *Oxid. Med. Cell. Longevity*, 2013, **2013**, 741817–741826.